

Frequency measurements in the $b\ ^3\Pi(0_u^+) - X\ ^1\Sigma_g^+$ system of K_2

I. Sherstov¹, S. Liu¹, Ch. Lisdat¹, H. Schnatz², S. Jung¹, H. Knöckel¹, and E. Tiemann^{1,a}

¹ Institut für Quantenoptik, Leibniz Universität Hannover, Welfengarten 1, 30167 Hannover, Germany

² Physikalisch-Technische Bundesanstalt, Bundesallee 100, 38116 Braunschweig, Germany

Received 17 November 2006

Published online 19 January 2007 – © EDP Sciences, Società Italiana di Fisica, Springer-Verlag 2007

Abstract. Absolute transition frequencies of the $b\ ^3\Pi(0_u^+) - X\ ^1\Sigma_g^+$ system of K_2 were measured in a molecular beam with Lamb dip absorption spectroscopy applying a frequency comb from a femtosecond pulsed laser. Both, K atoms and K_2 molecules are present in the beam and are expected to interact by collisions. The atoms can be deflected optically out of the beam, and thus the collision rate between K atoms and K_2 molecules is changed by about an order of magnitude. The molecular transition frequencies for low collisional rate are compared with those for high one. Limits for the collisional frequency shift within the beam are determined.

PACS. 33.20.Kf Visible spectra – 33.70.Jg Line and band widths, shapes, and shifts – 42.62.Fi Laser spectroscopy – 06.30.Ft Time and frequency

1 Introduction

The new and highly precise method of frequency measurement by means of a fs-laser frequency comb was applied to optical frequency standards like Ca [1], Sr^+ [2], Yb^+ [3] or Hg^+ [4] and also to precise determinations of other atomic transitions like for e.g. K [5] or Cs [6]. Here we want to extend it to a molecular case with K_2 . Caldwell et al. [7] about 20 years ago determined frequencies of several transitions in the $B\ ^1\Pi_u - X\ ^1\Sigma_g^+$ of K_2 with an accuracy of 2 parts in 10^{-9} by an interferometric method.

We shall here concentrate on very narrow spin forbidden transitions in the $K_2\ b\ ^3\Pi(0_u^+) - X\ ^1\Sigma_g^+$ spectrum, which we were able to observe recently [8,9]. Transitions in the $K_2\ b - X$ system gain some electric dipole strength due to admixture of the $A\ ^1\Sigma_u^+$ state to the b state via spin-orbit interaction. The relevant potential energy curves for K_2 are shown in Figure 1. The perturbed levels in the b state have long lifetimes of about $1\ \mu s$ and thus a narrow natural line width. Such transitions can be used for example as frequency references for other experiments with alkali atoms and molecules.

We used a femtosecond frequency comb referred to a commercial Cs atomic clock with an uncertainty below 10^{-11} in 1 s [10] to measure the absolute frequencies of molecular transitions. The potassium molecules were probed in a highly collimated potassium beam which significantly reduces the Doppler width of a molecular transition compared to cell experiments.

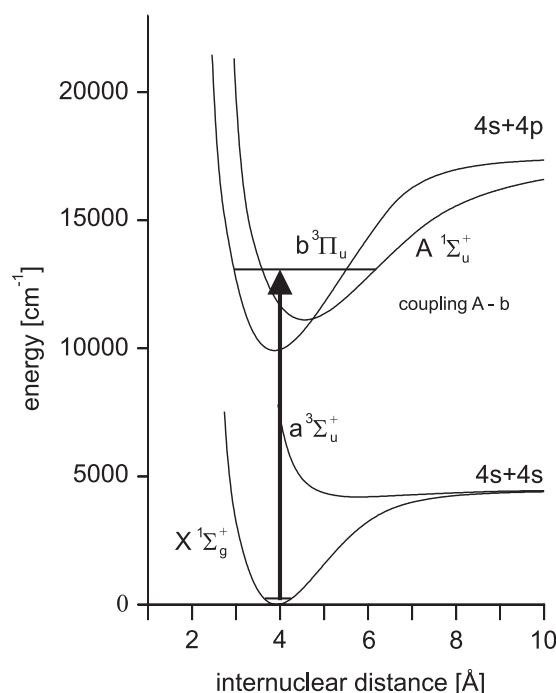


Fig. 1. Relevant potential energy curves of K_2 .

The molecular beam is created in an adiabatic expansion, which leads to a narrow velocity distribution of all constituents, namely atoms and dimers. Therefore, the collisions between atoms and molecules are addressed as being cold collisions, as their relative speed is on the order

^a e-mail: tiemann@iqo.uni-hannover.de

of 100 m/s. In contrast to cold collisions studied in traps, here the collision is taking place in a fast moving reference system, namely at the averaged speed of the atoms and molecules.

Highly precise frequency measurements of molecular lines with a fs-laser frequency comb, and especially difference frequency determinations, give a way to observe frequency shifts due to cold atom-molecule collisions in the potassium supersonic beam. We will vary the density of colliding particles within the beam to derive the collisional shift of the molecular transitions.

We first give a detailed outline of the experimental arrangement and the measurement procedure, then the evaluation of observed signals is described, followed by an analysis of the results. A discussion of the error budget and of relating the present results to other experiments closes the paper.

2 Experiment

2.1 Molecular beam

The molecular beam apparatus was already described in a previous paper [11]. Potassium metal is heated in a furnace and the vapor adiabatically expands out of a nozzle with diameter of 200 μm into the vacuum of the oven chamber. The central part of the expanding gas is guided through a skimmer (1) into the next vacuum chamber to form a particle beam. It consists mainly of K atoms and a small fraction of K_2 molecules. Typical particle velocities in the beam were determined by Doppler shift measurements to be about 950 m/s with a longitudinal velocity spread of about 150 m/s [11,12]. The overall collimation ratio of the beam through skimmer 2, which is located about 1 m downstream the beam path from the oven, with 2 mm diameter, is 1000 at the crossing with the spectroscopy laser beam. This gives a maximum residual Doppler effect in transverse direction of less than 1 MHz for the molecules at a laser wavelength of about 818 nm.

For the spectroscopy, the light of a frequency controlled tunable diode laser emerging out of a single mode fiber is polarized perpendicular to the particle beam and crosses at 90° angle the molecular beam. The sketch of the arrangement is shown in Figure 2. The laser beam is then retroreflected by a carefully interferometrically adjusted cat's eye made of an achromatic lens of 300 mm focal length and a mirror. The reflected beam crosses the molecular beam again at the same angle about 15 mm upstream the first crossing. The absorption due to the low molecular density in the potassium beam as well as losses on antireflection coated viewports of the beam chamber, the lens and mirror of the retroreflector can be neglected, so the intensities of the two counter propagating beams are practically equal. The laser induced molecular fluorescence is detected in a solid angle of 1.4 sr by a photomultiplier tube (Hamamatsu R 943-02) with an appropriate optical system. Tuning the laser frequency to resonance will deplete the population of the ground state level under consideration at crossing no. 1 in Figure 2, while the

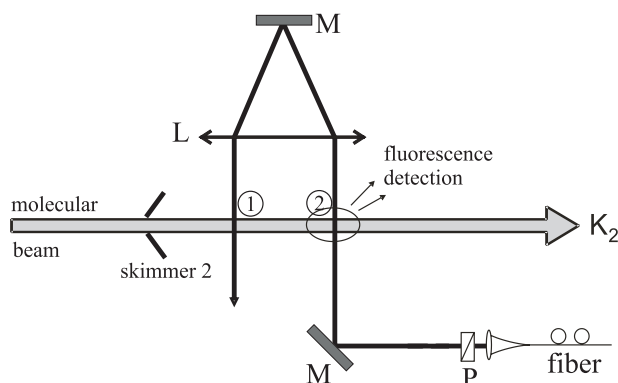


Fig. 2. The molecular beam setup for Lamb dip spectroscopy. P: polarizer, L: lens, M: mirror.

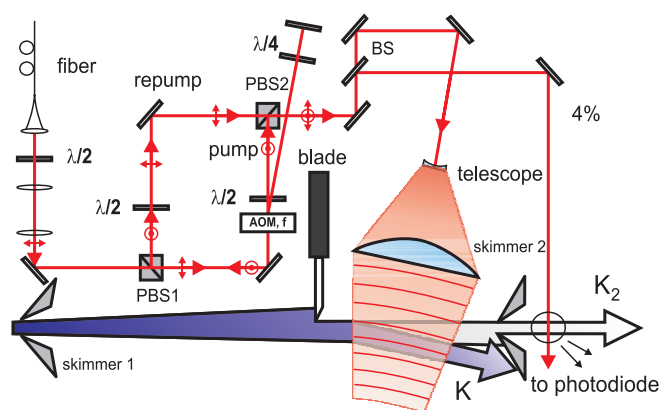


Fig. 3. Setup for the creation of the deflection laser fields. The wave fronts for the deflecting light are indicated. Polarization directions are indicated by arrows or circles with central dot. PBS: polarizing beamsplitter, $\lambda/4$: quarter wave plate, $\lambda/2$: half wave plate.

laser beam at crossing no. 2 detects the remaining population via laser induced fluorescence. The Doppler shifts of excitation in opposite directions are opposite. Thus, the spectral profile detected at crossing 2 will display a Lamb dip, which is at the center of the line for a well adjusted retroreflector and perpendicular crossing of the laser beams with the molecular beam. Uncertainties by residual Doppler shift due to uncertainties in the alignment will be discussed in Section 4.1.

2.2 Deflection of atoms

To change significantly the atom-molecule collisional rate, the atoms will be deflected out of the beam by resonant laser interaction through the $4s - 4p$ transition of K. A schematic overview of the optical setup for the generation of the deflection fields is shown in Figure 3. After about 50 cm of flight from the K-oven the particles pass a zone where the beam is shaped by a blade on one side and where laser fields of proper geometry and frequency can be applied to deflect the atoms such, that they do not pass through the second skimmer, which separates the vacuum chamber from the final UHV chamber (see the right part of

Fig. 3). There the particle beam is crossed with the beams of the spectroscopy laser. A small fraction (4%) of the light of the deflection laser crosses the particle beam about 40 cm downstream of the spectroscopy zone to probe the atoms remaining in the beam after the deflection.

For the deflection the atomic transition $^2S_{1/2}(f = 2) - ^2P_{3/2}(f' = 3)$ is employed. A repumper for the transition $^2S_{1/2}(f = 1) - ^2P_{3/2}(f' = 2)$ is necessary in order to obtain high efficiency of the deflection process. The arrangement for creation of these two light fields from a single titanium sapphire laser is also shown in Figure 3 and works as follows: the polarization of the light out of a single mode fiber is controlled by a $\lambda/2$ plate; the laser beam is shaped by a telescope and then guided through the polarizing beam splitter PBS1 to the acousto-optical modulator AOM. The zeroth diffraction order of the AOM goes to the polarizing beam splitter PBS2, while the first order is reflected back through the AOM with 90° rotated polarization and deflected from the incoming light by PBS1. Then the polarization is rotated again and the beam is superimposed with the zeroth order beam in PBS2. The AOM operates at 221.5 MHz, corresponding to half of the $(f = 1) - (f = 2)$ ground state hyperfine splitting minus half of the $(f' = 2) - (f' = 3)$ excited state hyperfine splitting of ^{39}K . While the laser is locked to a stabilized reference cavity and kept resonant with the $(f = 2) - (f' = 3)$ hyperfine component of the D2 line, the shifted frequency is resonant with the $(f = 1) - (f' = 2)$ transition and pumps back the atoms from the $f = 1$ ground state level to the $f = 2$ by optical pumping. Both laser fields illuminate the atom-molecule beam through an appropriate cylindrical optics, which is designed such that the deflected atoms follow the wavefronts for optimum deflection efficiency [13]. Regularly, more than 80% and in some cases up to 90% of the ^{39}K atoms are deflected out of the particle beam, which means a change in density by more than a factor of five.

2.3 Stabilized laser system for spectroscopy

The laser system for the spectroscopy of the molecular lines is based on a stabilized extended cavity diode laser (ECDL) and a slave laser for getting sufficient laser power. Figure 4 shows the schematic setup with an ECDL for 818 nm including a Pound-Drever-Hall (PDH) stabilization to a temperature stabilized confocal cavity ($\Delta T \approx 2$ mK) with 150 MHz free spectral range (FSR) and a finesse of 150. Long term stability of the cavity is obtained by locking the transmission peaks of the cavity via another diode laser operated at 780 nm to a saturated absorption peak of the Rb D2 line. The ECDL serves as a stabilized master laser for the spectroscopy. It has a line width of about 30 kHz and its long term drift is less than 300 Hz/min.

A fraction of the laser beam is guided in a double pass setup through an acousto-optical modulator. The frequency shifted laser field ν_{exp} is used for the injection lock of a diode laser called slave. Frequency tuning of the slave laser for spectroscopic purposes is obtained by tuning the

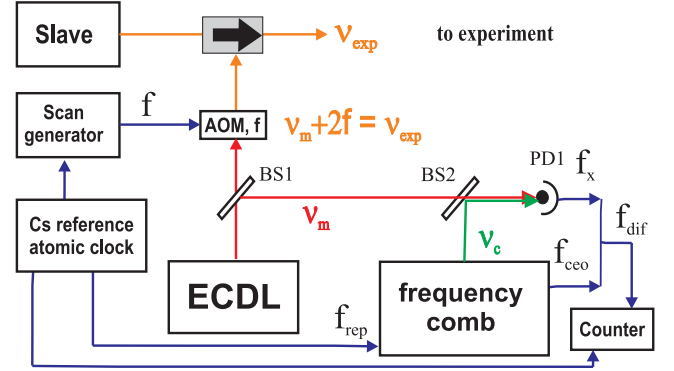


Fig. 4. Scheme of the laser stabilization of the laser used for spectroscopy.

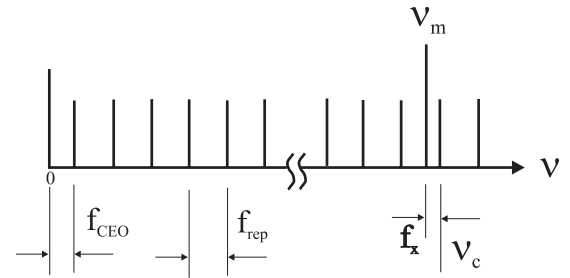


Fig. 5. Frequency scheme for determination of absolute frequencies with the frequency comb.

RF frequency f of the synthesizer which drives the AOM. The frequency of the synthesizer is phase locked to a Cs clock. Another fraction (about 3 mW) of the output of the ECDL is guided to the beam splitter BS2, where it is superimposed with the output spectrum of the self referenced optical frequency comb to obtain the beat frequency f_x on the photo diode PD1. For noise reduction and amplification of the beat frequency signal f_x we used a tracking oscillator.

2.4 Frequency comb

The basic function of a frequency comb from a femtosecond titanium sapphire pulsed laser is described in [10] and will not be detailed here. The repetition rate f_{rep} is counted with respect to a commercial Cs clock, which provides also the reference frequencies for all other oscillators involved in the frequency measurements. The principal scheme for the frequency measurement is shown in Figure 5. The carrier envelope offset frequency f_{CEO} is set such that the position of the first comb tooth is counted with $m = 0$, while f_{rep} was adjusted such that the nearest comb frequency ν_c is above the unknown optical frequency ν_m by an amount of f_x . The frequency ν_m of the ECDL is then calculated from the following formula:

$$\nu_m = m f_{rep} + f_{CEO} - f_x \quad (1)$$

where the definition of the frequencies is given in Figure 5 and m is the integer order of the comb tooth with

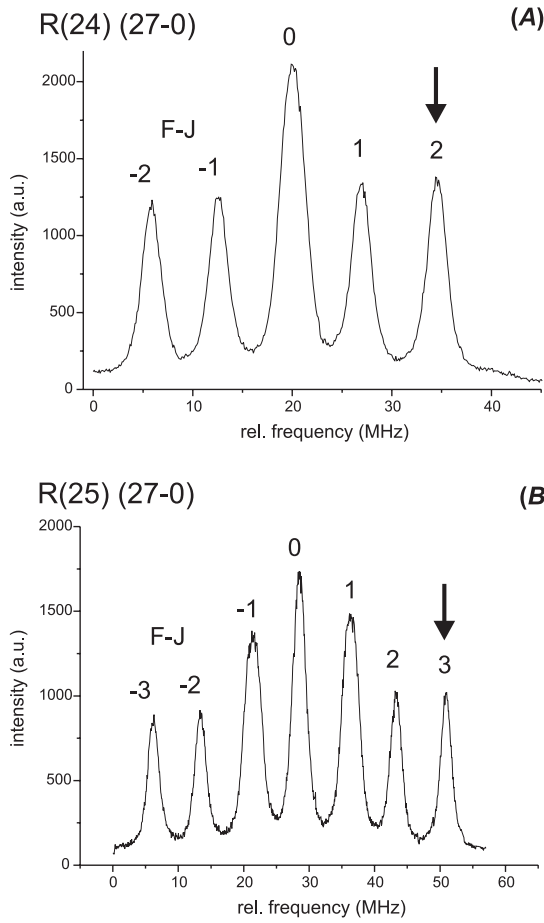


Fig. 6. Hyperfine spectrum of the R(24) (A) and R(25) (B) (27-0) lines of $b^3\Pi(0_u^+) - X^1\Sigma_g^+$ of K_2 . The retroreflector (see Fig. 2) was blocked for these records, so no Lamb dips appear.

frequency ν_c . As f_{rep} is around 700 MHz, m could be determined uniquely by a measurement of the molecular transition frequency with a commercial wavemeter, which is calibrated to an absolute accuracy of ± 100 MHz (High Finesse WS7).

The laboratory conditions caused a gradual drift of f_{CEO} which would limit the time of continuous measurement due to unlocking of the corresponding tracking oscillator. In the chosen configuration the drift of f_{CEO} results for a stable f_{rep} in a drift of f_x by the same amount. For better long term behavior we therefore mixed f_{CEO} and f_x , resulting in a difference frequency f_{dif} , which was counted employing a tracking oscillator. Finally, the frequency ν_{exp} of the slave laser is obtained by adding the frequency shift of the AOM, described in Section 2.3

$$\nu_{exp} = \nu_m + 2f = m.f_{rep} + f_{dif} + 2f. \quad (2)$$

During the experiment it was always cautiously checked that all frequencies are such that they enter with the signs given in formulas (1) and (2). The molecular beam spectra and the frequency trace for f were recorded continuously in equal time intervals with a data acquisition system. Synchronously f_{dif} and f_{rep} were recorded with another

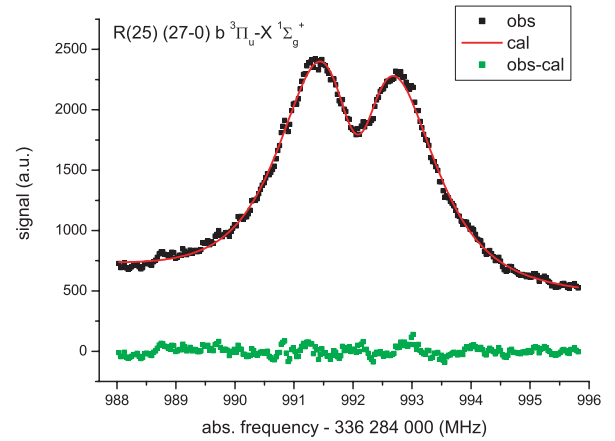


Fig. 7. Spectrum of the highest frequency hyperfine component of the R(24) (27-0) line of the $b^3\Pi(0_u^+) - X^1\Sigma_g^+$ system of K_2 . The Lamb dip in the line center has a width of about 500 kHz due to natural linewidth and transit time broadening.

data acquisition system on another time scale, together with f as marker used for later synchronization of both parallel records.

3 Measurements and results

As was already discussed in reference [9], lines of the $b^3\Pi(0_u^+) - X^1\Sigma_g^+$ system of K_2 display a splitting pattern, which is predominantly due to magnetic hyperfine structure. The number of hyperfine components depends due to the Pauli principle (nuclear spin 3/2 of ^{39}K and ^{41}K) for a homonuclear molecule on the rotational quantum number J'' for the ground state. For J'' even there are 6 components (total nuclear spin $I = 0$ and 2), while for J'' odd 10 components appear ($I = 1, 3$). A typical observed spectrum for even J'' is shown in Figure 6A where the central line is doubled and thus of higher intensity. Figure 6B shows the case of odd J'' . There the three central lines are doubled.

During the measurements, the master laser frequency was stabilized and measured with the comb, while the RF synthesizer for the slave laser was tuned across the molecular line. Typically a power of 3 mW was applied by a laser beam of about 2 mm diameter. For the recordings shown in Figure 6 the beam path through the retroreflector was blocked, so no depletion takes place and no Lamb dips appear.

For the frequency measurements we concentrated on the $F - J = +2$ and $F - J = +3$ hyperfine components of the R(24) and R(25) lines of the $b^3\Pi(0_u^+) - X^1\Sigma_g^+$ ($v' - v'' = (27-0)$ band, respectively (Fig. 6). The slave laser was tuned across an interval of about 10 MHz around the line center, in order to include also parts of the line wings of the neighboring line. In Figure 7 an example of such record is given. The central Lamb dip has a line width of about 500 kHz due to the natural linewidth ($\gamma_b = 150$ kHz) and transit time (about 2 μs) broadening.

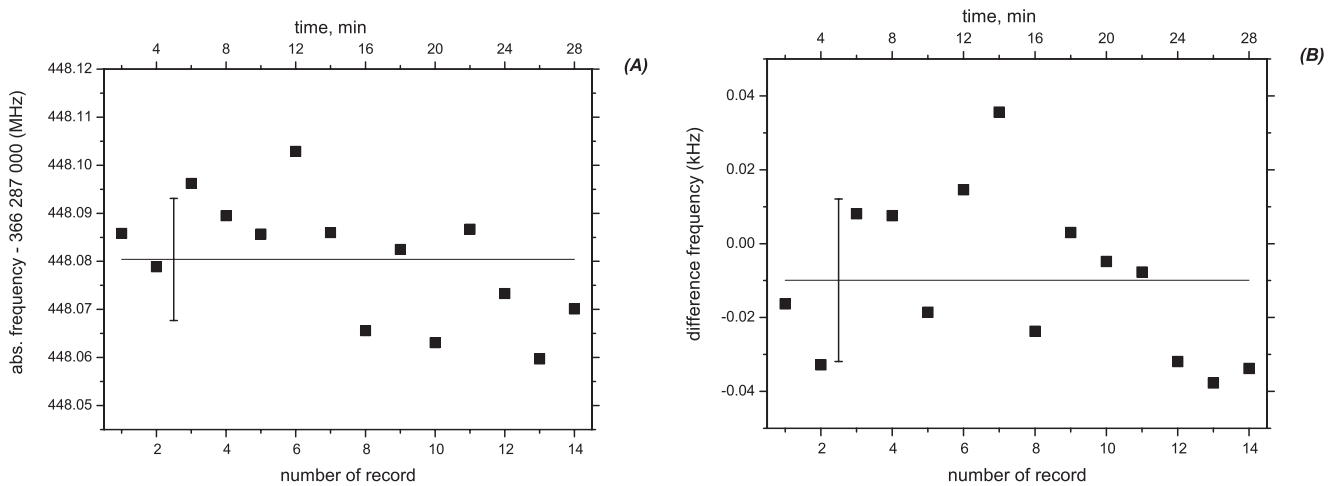


Fig. 8. Scatter of the measurement series corresponding to the 3rd row of Table 1 of the R(24) (27-0) line. Each scan result is obtained from a profile fit and an average of a pair of up and down scans. Panel (A) shows the results of records with low density of atoms. The horizontal line marks the average, and the error bar gives its standard deviation. Panel (B) shows the difference frequencies between the corresponding records with low and high densities of atoms. The horizontal line and the error bar mark the average and its standard deviation, respectively.

Spectra were recorded by tuning the laser stepwise with increasing frequency f across the structure and then with decreasing frequency back again to the starting frequency. In this manner one has always two spectra with opposite shifts due to time constants of the detection system. The step size was typically between 30 and 50 kHz per step with stepping time of 10 ms and integration time of 150 ms. The solid curve in Figure 7 is the result of fitting the observed signal with two superimposed profiles: an approximated Voigt profile for the hyperfine component and a Lorentzian for the Lamb dip. In the fitting procedure we also take into account a linearly varying frequency dependent background, which originates from superimposed wings of the neighboring hyperfine components. The fit residuals are shown in the lower part of Figure 7. They are small and do not show any systematic deviations.

Up to 30 samples of such frequency up/down pairs of spectra were collected, periodically changing the experiment from atoms being present in the particle beam for one sample to the case that atoms are deflected from the beam for the next sample. Several such measurements were collected for the R(24) and R(25) lines of the (27-0) band of the $b^3\Pi(0_u^+) - X^1\Sigma_g^+$ on different days.

We observed a systematic frequency shift of about 80 kHz between traces recorded with increasing and decreasing scanning frequency, which is expected by the fairly high ratio of the detection time constant and stepping time of 15:1. To correct for the effects of time constants, the frequencies determined by profile fitting of up and down scans were averaged pairwise. Because the line profile is not disturbed by the unfavorable time constant of the detection system we believe that averaging of up and down scans does not introduce errors larger than 10 kHz. Panel (A) in Figure 8 shows such frequencies of the Lamb dips of one of the longest measurement series of one day. The horizontal line gives the average, while the error bar marks its standard deviation. In panel (B) the differences

between corresponding records with low and high density of the atoms, together with their average and its standard deviation are shown.

The results of the absolute frequency measurements of the molecular lines for atomic density switched high/low in the experimental configuration described above are presented in Table 1. The absolute values for transition frequencies ν_{hi} for the case of high atomic density in the beam are listed in column 2, those for low atomic density (ν_{lo}) in column 3 of Table 1. The standard deviation in units of the last figure is given in brackets. Column 5 indicates the percentage of ^{39}K atoms deflected while in column 6 the number of recorded spectra yielding the frequencies in columns 2 and 3 is listed. Some large fluctuations in the value of the standard deviation of the absolute frequency measurements shown in Table 1 are caused by a poor number of averaged scans.

4 Discussion

4.1 Uncertainty budget

The precision of the described frequency measurements is limited by several effects, so we have to estimate their influence in the total uncertainty budget. The main uncertainty in the performed measurements is coming from the residual first order Doppler effect. For the implemented Lamb dip setup the parallelism of the counter propagating probe and saturation beams is determined by the alignment of the retroreflector. According to [14], the residual angle between the laser beams and the optical axis of the retroreflector can be derived from the uncertainty of the position of the mirror and estimated to be less than about $15 \mu\text{rad}$. This allows us to derive the contribution of the first order Doppler effect to the uncertainty of the absolute frequency measurements to be less than 34 kHz. For

Table 1. Results of absolute frequency measurements for two molecular lines. Always the hyperfine component with highest frequency is observed. The numbers in brackets give the 1σ standard deviation. If the density of the atoms was switched between records, the number of records for each experimental situation is given by the two numbers in column 6.

Molecular line	Absolute frequency, MHz		$\nu_{lo} - \nu_{hi}$ kHz	^{39}K atoms deflected %	Number of scans averaged
	high density of atoms	low density of atoms			
	ν_{hi}	ν_{lo}			
R(24) (27-0) $F - J = +2$	366 287 448.092(12)				7
	366 287 448.092(5)				5
	366 287 448.090(14)	366 287 448.080(10)	-10	83.6	14+14
	366 287 448.085(9)	366 287 448.085(11)	0	82.5	12+12
R(25) (27-0) $F - J = +3$	366 284 992.046(5)				3
	366 284 992.047(26)				3
	366 284 992.042(40)				2
	366 284 992.039(11)				4
	366 284 992.054(12)				6
	366 284 992.026(35)				3
	366 284 992.036(5)				3
	366 284 992.035(13)	366 284 992.031(13)	-4	81.8	5+5
	366 284 992.039(20)	366 284 992.050(14)	11	82.1	3+3
366 284 992.039(11)	366 284 992.040(11)	1	82.7	15+15	

the determination of frequency differences like search for the collisional shift we expect this effect to be significantly smaller because the optical alignment is the same for both classes of records and drifts are known to be small enough, because the thermal expansion, which is mainly responsible for possible drifts, of a 30 cm aluminium base of the retroreflector for a temperature fluctuations of <1 K in the lab during the recordings will lead to the frequency uncertainty of less than 12 kHz.

The second order Doppler shift for the frequency measurements was quite small. For the molecular velocity in the potassium beam of 950 ± 75 m/s it is calculated to be $-2.0(5)$ kHz and can be corrected.

The magnetic field is shielded in the interaction region by a μ -metal box. We determined the residual magnetic field to be less than 20 mG. Because the molecular states we measured are mainly non-magnetic (electronic angular momentum $\Omega = 0$) we can estimate the shift of a line to be less than 1 kHz because the effective g -factor is induced by rotation and should be in the order of the nuclear magneton [15].

The recoil by the absorption of the photon causes two systematic frequency shifts. The first one is shifting the line center by $\nu_r = h\nu^2/(2mc^2) \approx 3.8$ kHz. Here ν is the frequency of molecular transition, h is the Planck constant and m is the total mass of K_2 dimer. The second contribution would come from the average velocity $v_r = [h(\nu_m + \nu_r)/m]c \approx 0.7 \times 10^{-2}$ m/s the molecule gains per cycle of absorption and reemission. But according to the Franck-Condon principle, in our experiment we estimate with 98% probability that after one single excitation-spontaneous decay cycle molecules are lost for further excitation, and we have on average less than one photon scattered per molecule. Thus the frequency shift

caused by the total recoil effect can be estimated to be smaller than 4 kHz.

Following the arguments in [5], where highly precise frequency measurements of the D lines of potassium were performed, we assume that the ac-Stark effect in our frequency measurement does not give significant contribution to the uncertainty budget. The ac-Stark shift in our frequency measurement can be estimated from the formula

$$\Delta E_S = \frac{\Omega_0^2}{4\Delta E_{hf}} \quad (3)$$

where Ω_0^2 and ΔE_{hf} denote the Rabi frequency and hyperfine splitting of a molecular transition respectively. Due to the high rotational quantum numbers like $J = 24$ and 25 of the lines investigated here the hyperfine transitions observed obey the selection rule $F'' - F' = \Delta F = J'' - J' = \Delta J$, all other transitions with $\Delta F \neq \Delta J$ drop in intensity proportional to $1/(2J^2)$ or faster [15]. The ac Stark shift will influence the measured transitions due to near resonance of the laser frequency with $\Delta F = 0, \Delta J = \pm 1$ or $\Delta F = -\Delta J$ transitions sharing a common level with the measured one. Thus in spite of a relatively high laser intensity compared to [5] in our case we have much smaller transition moments for the hyperfine transitions and, moreover, a singlet-triplet electronic transition. So we estimate the ac-Stark shift of the molecular lines to be less than 1 kHz.

Another contribution to the uncertainty budget comes from the signal-to-noise ratio and thus the statistics of the recordings. The standard deviation of our measurements is given in Table 1 and is for long measurement series about 12 kHz.

The last contribution to the uncertainty budget stems from the frequency measurement by the comb. It gives

Table 2. Summary of the different contributions to the error budget excluding statistical uncertainty; in parenthesis error for difference measurements.

source	correction	uncertainty
First order Doppler effect	0.0 kHz	< 34 kHz
	(0.0 kHz)	(< 12 kHz)
Second order Doppler effect	2.0 kHz	0.5 kHz
	(0 kHz)	(< 0.1 kHz)
Zeeman effect	0 kHz	< 1 kHz
	(0 kHz)	(< 0.1 kHz)
ac-Stark effect	0 kHz	1 kHz
	(0 kHz)	(< 0.1 kHz)
Recoil shift	-3.8 kHz	0.5 kHz
	(0 kHz)	(< 0.1 kHz)
Time constant shift	0 kHz	10 kHz
	(0 kHz)	(1 kHz)
Frequency measurement		1 kHz
		(1 kHz)
	sum	sum
		in quadrature
for absolute measurements	-2 kHz	< 36 kHz
for difference measurements	(0 kHz)	< (12 kHz)

less than 1 kHz for the synchronized recording of comb frequency and molecular spectrum and the uncertainty of the Cs atomic clock.

The list of all contributions is presented in Table 2. Column 1 names the possible effects, while columns 2 and 3 show their contributions to the error budget for the correction and uncertainty of the frequency measurement, respectively. At the bottom of Table 2 the impact of all possible contributions to the correction and uncertainty is added up and their values are listed for absolute and difference frequency measurements.

4.2 Conclusion

The absolute frequencies of the lines R(24) and R(25) of the (27-0) band of the $b^3\Pi(0_u^+) - X^1\Sigma_g^+$ system stem from records taken during two days and show good consistency. The uncertainties excluding statistical contributions of the absolute and difference frequency measurements are 36 kHz and 12 kHz, respectively. The observed shifts between the line frequencies with high and low density of ^{39}K atoms listed in column 4 of Table 1 are results of various numbers of recordings. Thus we calculate the weighted average using as weights the number of records or its square root; both give a systematic shift of about -2 kHz. This we can take as the first indication that the collisional shift under these conditions is in the order of few kHz. The error budget shows, that this result despite the averaging is at the limit of the precision of our experimental setup. With further improvement on the experiment, especially the alignment responsible for the contribution of the Doppler effect, we might be able to detect this shift definitely.

The values of absolute frequencies for the $F - J = +2$ and $F - J = +3$ hyperfine components of the lines R(24) and R(25) of the $b^3\Pi(0_u^+) - X^1\Sigma_g^+$ (27-0) band shown in column 3 of table 1 were also weighted according to the corresponding number of records. The uncertainties include statistical contributions and the uncertainty from the error budget. The absolute frequency values are

$$\begin{aligned} \text{R(24)} (F - J) = +2 &\Rightarrow 366\,287\,448.082(37) \text{ MHz} \\ \text{R(25)} (F - J) = +3 &\Rightarrow 366\,284\,992.039(38) \text{ MHz.} \end{aligned}$$

The b-X transitions, selected according to their long lifetimes, are used for operating a matter wave interferometer (MWI) with K_2 molecules [11] in the same experimental setup. The MWI might be applied as another sensitive detector for the observation of weak interactions like cold collisions between K atoms and K_2 molecules in a supersonic beam. The idea is to observe the phase shift and the amplitude change induced by collisions in the interference pattern produced by weak interaction between potassium molecules and an environment like potassium atoms within the supersonic beam. A pioneering experiment with a similar goal was performed by the Pritchard group on Na_2 molecules, employing a MWI with nanofabricated gratings as beam splitters for the matter wave, where different target gases were introduced in one sufficiently widely separated arm of the interferometer [16,17]. We will employ a Ramsey-Bordé setup where two pairs of counterpropagating light fields are used as beam splitters for molecular matter waves and want to use this molecular MWI to observe with higher precision in-beam atom-molecule collisions, which from the present experiment are just at the limit to be detected.

The work is supported by DFG through SFB 407 and GRK 665. The authors thank A. Bauch from Physikalisch-Technische Bundesanstalt, Braunschweig, for the loan of the Cs-atomic clock.

References

1. C. Degenhardt, H. Stoehr, Ch. Lisdat, G. Wilpers, B. Lipphardt, T. Nazarova, P.-E. Pottie, U. Sterr, J. Helmcke, F. Riehle, Phys. Rev. A **72**, 062111 (2005)
2. H.S. Margolis, G.P. Barwood, G. Huang, H.A. Klein, S.N. Lea, K. Szymaniec, P. Gill, Science **306**, 1355 (2004)
3. J. Stenger, Chr. Tamm, N. Haverkamp, S. Weyers, H.R. Telle, Opt. Lett. **26**, 1589 (2001)
4. W.H. Oskay, S.A. Diddams, E.A. Donley, T.M. Fortier, T.P. Heavner, L. Hollberg, W.M. Itano, S.R. Jefferts, M.J. Delaney, K. Kim, F. Levi, T.E. Parker, J.C. Bergquist, Phys. Rev. Lett. **97**, 020801 (2006)
5. St. Falke, E. Tiemann, Ch. Lisdat, H. Schnatz, G. Grosche, Phys. Rev. A **74**, 032503 (2006)
6. V. Gerginov, K. Calkins, C.E. Tanner, J.J. McFerran, S. Diddams, A. Bartels, L. Hollberg, Phys. Rev. A **73**, 032504 (2006)
7. C.D. Caldwell, J. Jiménez-Mier, P. Zhao, F. Engelke, H. Hage, U. Schühle, J. Opt. Soc. Am. B **2**, 411 (1985)

8. Ch. Lisdat, O. Dulieu, H. Knöckel, E. Tiemann, Eur. Phys. J. D **17**, 319 (2001)
9. Ch. Lisdat, H. Knöckel, E. Tiemann, J. Mol. Spectr. **199**, 81 (2000)
10. H. Schnatz, B. Lipphardt, C. Degenhardt, E. Peik, T. Schneider, U. Sterr, Chr. Tamm, IEEE Trans. Instrum. Meas. **54**, 750 (2005)
11. Ch. Lisdat, M. Frank, H. Knöckel, M.-L. Almazor, E. Tiemann, Eur. Phys. J. D **12**, 235 (2000)
12. Ch. Lisdat: *Realisation eines Materiewelleninterferometers für Moleküle und neue Möglichkeiten zur Beobachtung von Atom-Molekül-Stößen*, Dissertation, Hannover 2001, available online at <http://www.tib.uni-hannover.de/webOPAC>
13. N. Nellesen, J.H. Müller, K. Sengstock, W. Ertmer, J. Opt. Soc. Am. B **6**, 2149 (1989)
14. K. Sengstock: *Ramsey Atominterferometrie an lasermanipulierten, kalten Atomen*, Dissertation, Bonn 1993, available at <http://www.ulb.uni-bonn.de/webOPAC>
15. C.H. Townes, A.L. Schawlow, *Microwave Spectroscopy* (Dover Publications Inc., 1975)
16. T.D. Hammond, M.S. Chapman, A. Lenef, J. Schmiedmayer, E.T. Smith, R.A. Rubenstein, D. Kokorowski, D.E. Pritchard, Braz. J. Phys. **27**, 193 (1997)
17. M.S. Chapman, C.R. Ekstrom, T.D. Hammond, R.A. Rubenstein, J. Schmiedmayer, S. Wehinger, D.E. Pritchard, Phys. Rev. Lett. **74**, 4783 (1995)